agronomy

MDPI

Article

Covalent Immobilisation of an *Aspergillus niger* Derived Endo-1,4-β-Mannanase, Man26A, on Glutaraldehyde-Activated Chitosan Nanoparticles for the Effective Production of Prebiotic MOS from Soybean Meal

Amy S. Anderson [1], Lithalethu Mkabayi [1], Samkelo Malgas [2], Naveen Kango [3] and Brett I. Pletschke [1,*]

[1] Enzyme Science Programme (ESP), Department of Biochemistry and Microbiology, Rhodes University, Makhanda 6140, South Africa
[2] Department of Biochemistry, Genetics and Microbiology, University of Pretoria, Hatfield 0028, South Africa
[3] Department of Microbiology, Dr Harisingh Gour Vishwavidyalaya (A Central University), Sagar 470003, India
* Correspondence: b.pletschke@ru.ac.za; Tel.: +27-46-603-8081

Abstract: An *Aspergillus niger* endo-1,4-β-mannanase, Man26A, was confirmed by FTIR and XRD to be immobilised on glutaraldehyde-activated chitosan nanoparticles via covalent bonding. The immobilisation (%) and activity yields (%) were 82.25% and 20.75%, respectively. The biochemical properties (pH, temperature optima, and stability) were then comparatively evaluated for both the free and immobilised Man26A. The optimal activity of Man26A shifted to a lower pH after immobilisation (pH 2.0–3.0, from pH 5 for the free enzyme), with the optimum temperature remaining unchanged (60 °C). The two enzymes exhibited identical thermal stability, maintaining 100% activity for the first 6 h at 55 °C. Substrate-specific kinetic analysis showed that the two enzymes had similar affinities towards locust bean gum (LBG) with varied V_{max} values. In contrast, they showed various affinities towards soybean meal (SBM) and similar V_{max} values. The immobilised enzyme was then employed in the enhancement of the functional feed/prebiotic properties of SBM from poultry feed, increasing mannooligosaccharides (MOS) quantities. The SBM main hydrolysis products were mannobiose (M2) and mannose (M1). The SBM-produced sugars could be utilised as a carbon source by probiotic bacteria; *Streptococcus thermophilus*, *Bacillus subtilis*, and *Lactobacillus bulgaricus*. The results indicate that the immobilised enzyme has the potential for use in the sustainable and cost-effective production of prebiotic MOS from agricultural biomass.

Keywords: chitosan; endo-1,4-β-mannanase; immobilisation; mannooligosaccharides; prebiotic; soybean meal

Citation: Anderson, A.S.; Mkabayi, L.; Malgas, S.; Kango, N.; Pletschke, B.I. Covalent Immobilisation of an *Aspergillus niger* Derived Endo-1,4-β-Mannanase, Man26A, on Glutaraldehyde-Activated Chitosan Nanoparticles for the Effective Production of Prebiotic MOS from Soybean Meal. *Agronomy* **2022**, *12*, 2993. https://doi.org/10.3390/agronomy12122993

Academic Editors: Carlos Martín and Eulogio Castro

Received: 20 October 2022
Accepted: 23 November 2022
Published: 28 November 2022

1. Introduction

In recent years, oligosaccharides have been gaining much attention from researchers in various fields. Many oligosaccharides have been reported to possess prebiotic properties and are highly important in various industries, including feed, food, and pharmaceuticals [1]. A prebiotic is a non-digestible food component that selectively stimulates the growth or activity of one or a limited number of indigenous bacteria (probiotics) in the digestive tract in a manner claimed to be beneficial for the host [2,3]. Different types of oligosaccharides are recognised as prebiotics. Among these, hemicellulose-derived oligosaccharides, such as xylooligosaccharides (XOS) and MOS, have garnered much attention as they can be easily generated from various agricultural residues that are low-cost substrates [1]. MOS derived from different mannan-containing raw feedstocks have excellent potential as ideal candidates for new-generation prebiotics [4]. Several studies have reported that MOS supplementation could improve various animals' growth performance and immune response [5–7]. In animals such as broilers and pigs, MOS appear to improve health by changing the bacterial ecology of their guts.

B-MOS are generally prepared by hydrolysis of mannan, a heteropolysaccharide mainly composed of repeating units of mannopyranoside residues linked by β-1,4-glycosidic linkages. These chains can contain 1–10 mannose residues, creating a linear chain which can be further classified as α-/β-MOS—this being determined by the source of the mannans the MOS was derived from [1]. Mannans are classified as linear mannan, glucomannan, galactomannan, and galactoglucomannan [8]. Mannans, mainly galactomannan, are also found in SBM, a primary source of plant protein used in poultry feed [9]. Previous studies demonstrated that the amount of mannan is between 1.33 and 2.14% in non-dehulled SBM and 1.02 and 1.51% in dehulled SBM [10]. The presence of mannan in SBM may negatively affect nutrient utilisation and poultry performance [11]. Therefore, hydrolysis of mannan in SBM leads to the release of prebiotic MOS that can enrich the growth of health-promoting gut microbiota in poultry while improving nutrient digestibility [12]. Within mannan hydrolysis, by an endo-1,4-β-mannanase, favourable by-products focus specifically on producing β-1,4-mannobiose. This MOS residue has proven to be specifically beneficial in depleting the quantities of pathogenic bacteria, such as *Salmonella enterica*, in the gastrointestinal tract of poultry [12].

Increasing evidence suggests that the application of enzymes can improve the nutritional value of SBM-based diets [13,14]. The enzyme mainly used in this process, endo-1,4-β-mannanase, is found in various sources, such as bacteria, fungi, and yeasts [15]. Endo-1,4-β-mannanase (EC 3.2.1.78), also called 1,4-β-D-mannan mannanohydrolase, is a glycoside hydrolase (GH), specifically an endo-hydrolase [16]. This enzyme is mainly responsible for the random cleavage of internal β-1,4-glycosidic bonds in the backbone of mannans to yield MOS [8]. Mannanases belong to GH clan A, under families GH5, GH26, GH45, GH113, and GH134 (www.cazy.org (accessed on 19 October 2022)). The enzymatic hydrolysis of mannans results in the production of β-MOS which possesses the essential characteristics of prebiotics. These include a short degree of polymerisation (DP < 4), resistance to gastrointestinal (GI) enzymes, stability in gastric juice, and selective utilisation by probiotics [7,17,18].

Despite their numerous advantages, the practical application of enzymes has often been hampered by several limitations, including non-reusability and the lack of long-term operational stability due to sensitivity to denaturation [19]. These challenges can be overcome by immobilising the enzymes onto solid carriers. Compared to free enzymes, immobilised enzymes offer many advantages, such as ease of recovery from the reaction mixture, thus facilitating their reuse, enhanced stability, rapid termination of reactions, and simplified product purification process [20,21]. The immobilisation of enzymes onto carriers can be achieved using various methods, broadly categorised into physical adsorption, entrapment in a matrix, ionic binding, covalent binding, and cross-linking [22]. These strategies have gained increasing interest, as enzymes in industrial settings are associated with high costs, instability, and high loading demands [22]—therefore, immobilisation of enzymes has provided an efficient method for biocatalyst recycling. Chitosan is often preferred among the best-known carriers because of its abundance, biocompatibility, thermal and chemical stability, and nontoxicity [19,22]. Chitosan is a polyaminosaccharide produced through the deacetylation of chitin [23]. The presence of multiple reactive functional groups on the chitosan surface can facilitate efficient binding between chitosan and the enzyme. This is generally done by treating chitosan with a bi-functional reagent, such as glutaraldehyde, which forms covalent bonds with amino groups on the chitosan surface and the enzyme [24]. Several studies have demonstrated the immobilisation of enzymes on chitosan-based supports for applications in various reactions [25–28].

This study describes the immobilisation of an endo-1,4-β-mannanase, Man26A, derived from *Aspergillus niger* on glutaraldehyde-activated chitosan nanoparticles. The characteristics of the immobilised and free endo-1,4-β-mannanase were compared and the applicability of the immobilised enzyme in MOS production from SBM was demonstrated. This work investigates improving the quality of SBM ingested by monogastric animals, specifically poultry, by testing a recyclable enzymes efficacy against the complex sub-

strate SBM—in addition, the potential in vitro prebiotic activity of the generated MOS was confirmed using selected probiotic bacterial species.

2. Materials and Methods

2.1. Materials

The mannobiose (M2), mannotriose (M3), mannotetraose (M4), mannopentaose (M5), mannohexaose (M6), galactosyl-mannotriose (G-M3), di-galactosyl-mannopentaose (G2-M5), and endo-1,4-β-mannanase (Man26A) derived from *A. niger* were purchased from Megazyme (Bray, Wicklow, Ireland). SBM was purchased from Rayner general agencies (Makhanda, EC, South Africa). The Carbosep CHO 411 column was purchased from Concise Separations (San Jose, CA, USA). All other chemicals used in the study were purchased from Sigma-Aldrich (St. Louis, MO, USA).

2.2. Preparation of Chitosan Nanoparticles

Glutaraldehyde-activated chitosan nanoparticles were prepared according to a previously described method [29] with slight modifications. Chitosan (0.25% w/v) was suspended in 50 mM citrate buffer (pH 5.0) with 1% (v/v) Tween 80, and 0.35 M acetic acid, and the mixture was stirred (150 rpm) for 20 min at 30 °C. Under sonication, using a Vibra-Cell™ (20 kHz at an amplification of 60), 1.4 M sodium sulphate solution was added dropwise to the chitosan mixture and then stirred magnetically (2 h, 500 rpm). Particles were then collected via centrifugation using a 1.0R Megafuge (3500× g, 15 min, 4 °C) and washed with deionised water (3500× g, 15 min, 4 °C). The particles were activated under agitation by the addition of 1.25% (v/v) glutaraldehyde in 50 mM citrate buffer (pH 5.0) (30 °C, 45 min). The activated chitosan nanoparticles were washed several times to remove excess glutaraldehyde (3500× g, 10 min, 4 °C).

2.3. Immobilisation of Man26A on Chitosan Nanoparticles

The washed, activated nanoparticles were then incubated with a 0.1 mg/mL enzyme solution of endo-1,4-β-mannanase, Man26A (36 h, 4 °C). After the incubation time had elapsed, the immobilised enzyme was washed several times (3500× g, 10 min, 4 °C). Each wash was tested for protein concentration (as described in Section 2.5.1) and reducing sugar concentration (as described in Sections 2.5.2 and 2.5.3) to assist in the calculation of the immobilisation yield. The immobilised enzyme was stored at 4 °C until further use.

The Immobilisation yield was expressed as described previously by [29].

$$Immobilisation\ yield = \frac{A - B}{A} \times 100 \quad (1)$$

The activity yield was defined according to the following expression previously described by [29]:

$$Activity\ yield\ (\%) = \frac{Specific\ Activity\ of\ the\ immobilised\ enzyme}{Specific\ Activity\ of\ the\ Free\ Enzyme} \times 100 \quad (2)$$

(A): the quantity of enzyme loaded for immobilisation procedure (mg); (B): unbound protein after immobilisation (mg); and (A–B): the theoretical immobilised enzyme.

2.4. Bio-Physical Characterisation of Man26A-Immobilised Chitosan Nanoparticles

2.4.1. FTIR Analysis

A spectrum 100 Fourier-transform infrared spectroscopy (FTIR) system (Perkin Elmer, Wellesley, MA, USA) was used to characterise untreated chitosan, glutaraldehyde-activated chitosan nanoparticles, and the Man26A-immobilised chitosan nanoparticles. Each sample dried using critical point drying was pressed uniformly against the sample spotting surface using a spring-loaded anvil. FTIR spectra were obtained from scans from 4000 to 600 cm^{-1}.

Baseline and ATR corrections for penetration depth and frequency variations were carried out using the SpectrumOne^{TM} software supplied with the equipment.

2.4.2. XRD Analysis

Samples of chitosan, glutaraldehyde-activated chitosan, and endo-1,4-β-mannanase immobilised on glutaraldehyde-activated chitosan nanoparticles were analysed via an X-ray diffractometer (XRD) (Bruker D2 Phaser, Karlsruhe, Germany). This was done with a LYNXEYE XE-T detector using Cu radiation (wavelength λ = 0.154 A°) at a voltage of 30 kV on a current of 10 mA. The samples were scanned from 2θ of 5 to 60° with a step size of 0.02°. The determination time was 0.02° per second.

2.5. Determination of Enzyme Activity and Protein Concentration

2.5.1. Protein Concentration

A Bradford's assay was used to determine the protein concentration of the endo-1,4-β-mannanase, using bovine serum albumin (BSA) as a suitable standard [30]. The protein samples were combined with Bradford's working reagent in a 1:9.2 ratio. The readings were taken after 10 min on a Synergy MX microplate reader (BioTek, Winooski, VT, USA) at a wavelength of 595 nm.

2.5.2. Determination of Reducing Sugars Concentration

The endo-1,4-β-mannanase activity was assayed by quantitatively measuring the amount of reducing sugars released in a hydrolysis reaction using the 3,5-dinitrosalicylic acid (DNS) method described previously [31], with modifications. DNS reagent (1% *w*/*v* NaOH, 1% *w*/*v* 3,5-dinitrosalicylic acid, 20% *w*/*v* potassium sodium tartrate tetrahydrate, 0.2% *w*/*v* phenol, 0.05% *w*/*v* sodium metabisulphite) was combined with reducing sugar sample in a 2:1 ratio, respectively. The samples were then incubated at 100 °C for 6 min, and the absorbance was read on a Synergy MX microplate reader (BioTek, Winooski, VT, USA) at 540 nm. A standard curve was prepared using mannose as a suitable standard (0.1–1.2 mg/mL).

2.5.3. Endo-1,4-β-mannanase Activity Assay with LBG

The activity of endo-1,4-β-mannanase was determined using the model substrate, 0.5% (*w*/*v*) LBG, in 50 mM citrate buffer (pH 5.0) [8]. The reaction was conducted at 55 °C for 30 min. The enzymatic activity was terminated by incubation at 100 °C for 5 min, followed by centrifugation at 16,000× *g* for 5 min. The enzyme activity was determined by measuring the amount of reducing sugars produced (as described in Section 2.5.2). One unit of enzyme activity was defined as the amount of enzyme that released 1 µmol of reducing sugars per minute under the assay conditions specified. All assays were performed in triplicate, and average values were reported.

2.5.4. Endo-1,4-β-mannanase Activity Assay with SBM

The activity of endo-1,4-β-mannanase was determined using a 6% (*w*/*v*) SBM in 50 mM citrate buffer (pH 5.0). The reaction was conducted at 55 °C for 48 h, with 1.5-h prewetting at 90 °C. The enzymatic activity was terminated by incubation at 100 °C for 5 min, followed by centrifugation at 16,000× *g* for 5 min. The enzyme activity was determined by measuring the amount of reducing sugars produced (as described in Section 2.5.2). One unit of enzyme activity was defined as the amount of enzyme that released 1 µmol of reducing sugars per minute under the assay conditions specified. All assays were performed in triplicate, and average values were reported.

2.6. Biochemical Characterisation of Free and Immobilised Man26A

2.6.1. Temperature Optima

To determine the effect of temperature, the activities of the free enzyme (44.05 U/mg) and immobilised enzyme (9.14 U/mg) were tested at temperatures ranging from 30–80 °C

at intervals of 10 °C. The residual activity was measured at specific time intervals under the standard assay conditions (as described in Section 2.5.3) and analysed by the DNS method (Section 2.5.2). The maximal enzyme activity in each experiment was expressed as 100% activity, which allowed the mannanase activity to be expressed as a relative percentage of its maximal activity.

2.6.2. Thermostability Determination

The temperature effect on enzyme stability was determined at 55 °C during a period ranging from 0–72 h. Both free (44.05 U/mg) and immobilised enzyme (9.14 U/mg) preparations were incubated in 50 mM citrate buffer (pH 5.0) at the temperature specified above. The residual activity was measured at specific time intervals under the standard assay conditions (as described in Section 2.5.3) and analysed by the DNS method (Section 2.5.2). The maximal enzyme activity in each experiment was expressed as 100% activity, which allowed the mannanase activity to be expressed as a relative percentage of its maximal activity.

2.6.3. PH Optima

The activity of the free (44.05 U/mg) and immobilised (9.14 U/mg) endo-1,4-β-mannanase derived from *A. niger* was assayed at different pH values (2–9) using a universal buffer [32]. A mannanase activity assay was conducted (as described in Section 2.5.3) and analysed by the DNS method (Section 2.5.2). The maximal enzyme activity in each experiment was expressed as 100%, which allowed the mannanase activity to be described as a relative percentage of its maximal activity.

2.6.4. Kinetic Parameters of Immobilised and Free Endo-1,4-β-mannanase with LBG

The kinetic parameters were determined for the model substrate LBG in the concentration range of 0.5–15 mg/mL in 50 mM citrate buffer (pH 5.0), the complex substrate SBM in the concentration range of 30–80 mg/mL in 50 mM citrate buffer (pH 5.0), with assay conditions as described in Sections 2.5.3 and 2.5.4, respectively. The Michaelis–Menten constant, K_M, and maximum rate, V_{max}, were determined using non-linear regression analysis with GraphPad Prism 6.0 software.

2.7. Reusability of the Immobilised Man26A

The chitosan-immobilised endo-1,4-β-mannanase (0.02 g) was weighed and resuspended in 100 µL of 50 mM citrate buffer (pH 5.0). A reaction was then conducted according to Section 2.5.3. At the end of the reaction, the immobilised mannanase was recovered by centrifugation (16,000× *g*, 5 min) and was rinsed thrice with 50 mM citrate buffer (pH 5.0). Next, fresh 0.5% (*w*/*v*) LBG was added, and the activity was tested again according to Section 2.5.3. After each cycle, the reducing sugar concentration produced by the immobilised mannanase was determined. All reactions were prepared in technical duplicates and biological triplicates.

2.8. HPLC Analysis of MOS Generated from SBM

For HPLC analysis, the following MOS standards were prepared at 0.01% (*w*/*v*); mannose, mannobiose, mannotriose, mannotetraose, mannopentaose, and mannohexaose. The HPLC-RID Shimadzu system (Shimadzu Corp, Kyoto, Japan) was set up using a CarboSep CHO 411 column. Deionised water was used as the mobile phase in isocratic mode at a flow rate of 0.3 mL/min, and the column temperature was set at 80 °C. All samples and MOS standards used an injection volume of 20 µL.

2.9. Prebiotic Effects of SBM-Derived MOS

2.9.1. Bacterial Culture

The prebiotic activity of endo-1,4-β-mannanase-generated sugars was evaluated according to the previously described method [33]. In vitro fermentation of the prebiotic sugars was carried out by probiotic bacteria (*Streptococcus thermophilus*, *Bacillus subtilis*,

and *Lactobacillus bulgaricus*) grown in 1 × M9 minimal media (2.5 g/L NaCl, 5 g/L NH_4Cl, 15 g/L KH_2HPO_4 (pH 7.4)). Each strain was inoculated to an initial absorbance (OD_{600}) of 0.1 and cultivated at 37 °C for 6 h. Batch fermentation was carried out in an M9 medium supplemented with 0.0155% MOS and 1 mg/mL glucose as a positive control. A negative control, without a carbon source, was also prepared, and all the experiments were completed twice (biological replicates) in triplicate (technical replicates).

2.9.2. Effects of MOS on Cell Viability

The viability of the cultured bacterial cells was determined by adding 50 µL of 0.02% (*w*/*v*) of *p*-iodonitrotetrazolium chloride (INT) into a 96-well microtiter plate (Lasec, Cape Town, WC, South Africa) containing 200 µL of the cultured bacterial sample. The plate was incubated for 1 h at 27 °C, and the absorbance was measured at 490 nm using a Synergy MX microplate reader (Biotek, Winooski, VT, USA).

Cell density was established by centrifuging (16,000× *g*, 3 min) 1 mL of bacterial sample, removing the supernatant, and resuspending in 250 µL of phosphate buffer (pH 7.4). The samples were placed in a 96-well microtiter plate, and the absorbance (OD_{600}) was measured using a Synergy MX microplate reader.

2.10. Statistical Analysis

All data that are presented represent the means and standard deviations (SD) of triplicates. A *t*-test was used to analyse all data using GraphPad Prism 6.0 software. A *p*-value of less than 0.05 indicated statistically significant differences between the compared datasets.

3. Results

3.1. Enzyme Immobilisation

Enzyme immobilisation and activity yields were calculated according to Section 2.3. Immobilisation was achieved for chitosan with an immobilisation yield of 82.25%. The specific activities of the immobilised enzyme on LBG were low compared to that of the free enzyme (44.05 U/mg), with chitosan displaying a 9.14 U/mg specific activity. The immobilisation yields of the β-mannanase on chitosan were highly successful, although the activity yields showed that the binding was unproductive. Chitosan immobilised endo-1,4-β-mannanase reached a 20.75% yield in activity.

3.2. Bio-Physical Characterisation of Immobilised Chitosan Nanoparticles

3.2.1. FTIR Spectroscopy

The FTIR spectra of untreated chitosan beads (chitosan), glutaraldehyde-activated chitosan nanoparticles (A-CTS), and endo-1,4-β-mannanase-immobilised glutaraldehyde-activated chitosan nanoparticles (CTS) can be seen in Figure 1. The identified peaks were studied to perform the in situ analysis of the chitosan surface for investigating the surface adsorption of functional groups due to the glutaraldehyde activation and the enzyme immobilisation procedure. FTIR analysis of chitosan showed characteristic bands at 3276 cm^{-1} (-OH stretching band), 2961 cm^{-1} (-CH stretching region), 2915 cm^{-1} (-NH), and bands at 1642 cm^{-1} and 1604 cm^{-1} ($-NH_2$). The A-CTS sample showed bands present at 3260 cm^{-1} (-OH stretching vibration), 2967 cm^{-1} (-CH stretching region), 2915 cm^{-1} (-NH), 1730 cm^{-1} (-C=O), 1681 cm^{-1} and 1687 cm^{-1} (-C=N). The CTS sample experienced prominent bands at 3206 cm^{-1} (-OH stretching vibrations), 2987 cm^{-1} (-CH stretching region), 2910 cm^{-1} (-NH), 1730 cm^{-1} (-C=O), 1685 cm^{-1}, and 1697cm^{-1} (C=N).

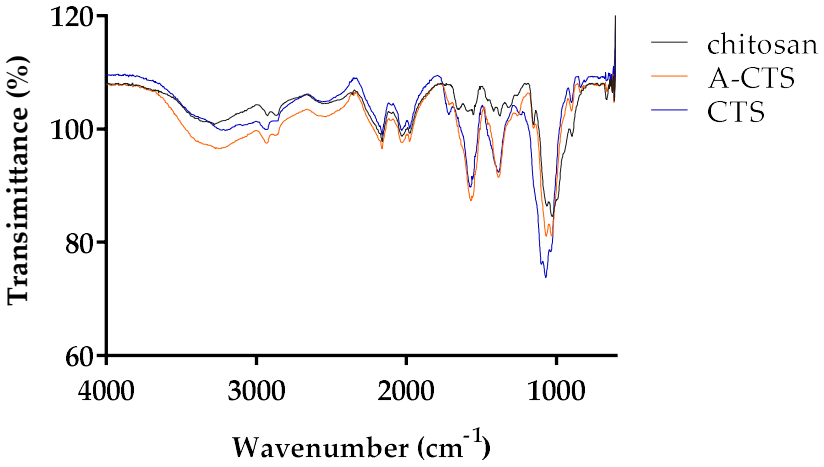

Figure 1. Comparison of FTIR spectra of Chitosan, A-CTS, and CTS. FTIR spectra were obtained from scans from 4000 to 600 cm^{-1}.

3.2.2. X-ray Diffraction Analysis

XRD was used to investigate the change in chitosan's structure after glutaraldehyde activation and enzyme immobilisation. The XRD pattern of chitosan (Figure 2a) showed two distinctive crystallinity peaks at 2θ = 10.558° and 19.661° associated with 020 and 110 planes of the crystallite, respectively. The morphology of the chitosan was altered after activation with glutaraldehyde, this can be seen by the drastic drop in intensity with low peaks associated with crystallinity of the biomass. Furthermore, the addition of Man26A to the surface of the glutaraldehyde-activated chitosan led to the re-emergence of the 2θ = 20° peak; however, it was broad, this supporting evidence of immobilisation in an ordered amorphous manner.

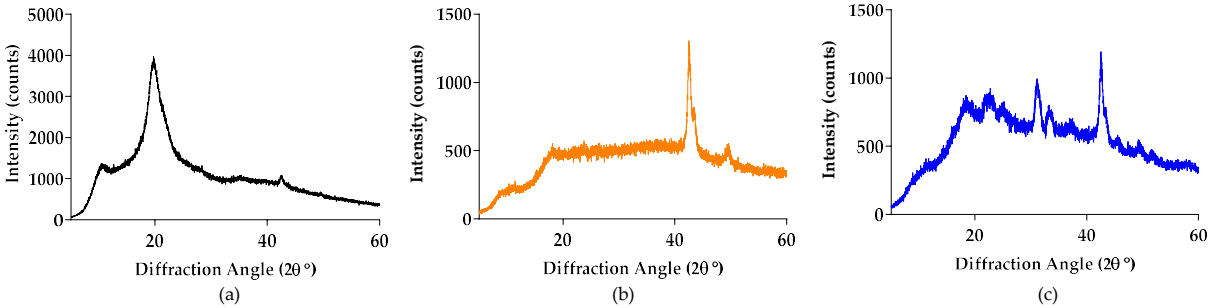

Figure 2. X-ray diffraction patterns of (**a**) chitosan, (**b**) glutaraldehyde-activated chitosan nanoparticles, and (**c**) endo-1,4-β-mannanase immobilised on glutaraldehyde-activated chitosan nanoparticles.

3.3. Biochemical Characterisation of Free and Immobilised Man26A

3.3.1. Effect of Temperature and pH on Enzyme Activity

The effect of temperature on the free and immobilised endo-1,4-β-mannanase indicated that both enzymes had a similar optimum temperature of 60 °C (Figure 3a). Furthermore, during thermostability determination, the activity of both the immobilised and free enzyme increased over the first 10 h of incubation; thereafter, it decreased to approximately 75%. After 72 h of incubation, the immobilised and free enzymes retained 18% and 12% of their relative activity, respectively.

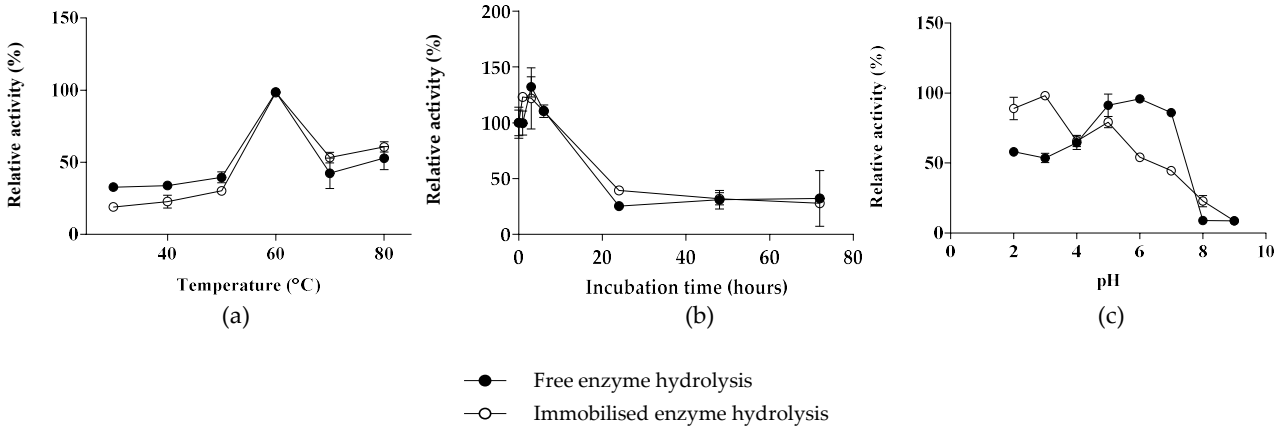

Figure 3. (**a**) Temperature optimum (30–80 °C), (**b**) thermostability (0–72 h), and (**c**) pH optimum study of immobilised (9.14 U/mg) and free (44.05 U/mg) endo-1,4-β-mannanase under hydrolysis with 0.5% (*w*/*v*) LBG (30-min, 55 °C).

As shown in Figure 3, the optimum pH of the free enzyme shifted from its optimal neutral pH (5–7) to a more acidic pH of 2–3 for the immobilised enzyme. The immobilised endo-1,4-β-mannanase retained a higher relative activity below pH 4.

3.3.2. Kinetic Parameters

Under the optimal assay conditions, free and immobilised endo-1,4-β-mannanase were evaluated for kinetic parameters against LBG (Figure 4a) and SBM (Figure 4b). The LBG kinetics study for free and immobilised endo-1,4-β-mannanase exhibited K_M and V_{max} values of 8.44 mg/mL and 55.36 U/mg-protein, and 7.74 mg/mL and 12.10 U/mg, respectively (Figure 4a and Table 1). The k_{cat} values of the immobilised and free enzymes differed significantly, showing 322.6 s^{-1} and 5536 s^{-1}, respectively. The kinetic parameters against SBM (Figure 4b and Table 1) for the free and immobilised enzyme exhibited K_M and V_{max} values of 53.43 mg/mL and 0.03099 U/mg, and 10.26 mg/mL and 0.02672 U/mg, respectively. The k_{cat}/K_m favoured the immobilised enzyme reaction (0.0981 s^{-1} mg^{-1} mL) when hydrolysing SBM as the substrate.

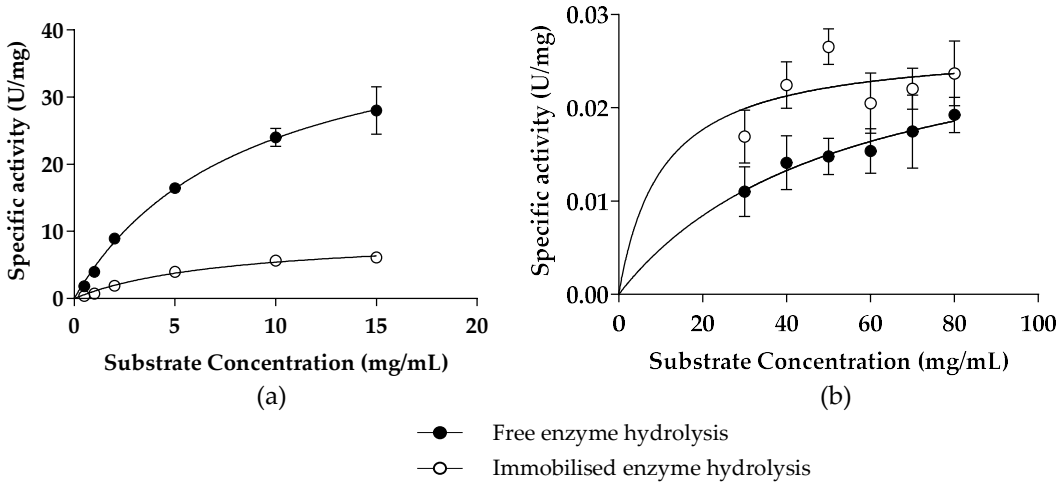

Figure 4. Michaelis–Menten kinetics of free and immobilised endo-1,4-β-mannanase hydrolysing (**a**) LBG (0.5–15 mg/mL) (30-min, 55 °C) and (**b**) SBM (30–80 mg/mL) (48 h, 55 °C). The kinetic parameters were determined at the optimal pH and temperature for both enzymes. The values were presented as mean ± SD (n = 3).

Table 1. Kinetic parameters of free and immobilised endo-1,4-β-mannanase with LBG (0.05–0.15% (*w*/*v*)) and SBM (3.0–8.0% (*w*/*v*)).

Substrate	Kinetic Parameters	Immobilised Enzyme	Free Enzyme
LBG	V_{max}	12.10	55.36
	K_m (mg/mL)	7.74	8.44
	k_{cat} (s^{-1})	322.6	5536.0
	k_{cat}/K_m (s^{-1} mg^{-1} mL)	41.67	655.85
SBM	V_{max}	0.02672	0.03099
	K_m (mg/mL)	10.26	53.43
	k_{cat} (s^{-1})	1.006	0.6199
	k_{cat}/K_m (s^{-1} mg^{-1} mL)	0.0981	0.0116

3.4. Reusability of the Immobilised Man26A

Endo-1,4-β-mannanase was immobilised on chitosan-activated nanoparticles, facilitated by 1.25% (*v*/*v*) glutaraldehyde, as described by [28], as stated in Sections 2.2 and 2.3. The reusability was analysed against the model substrate 0.5% (*w*/*v*) LBG (30 min, 55 °C), which produced 0.960 mg/mL of reducing sugars after cycle 1. Reducing sugar production by the immobilised enzyme dropped to 0.545 mg/mL by the 9th cycle. This showed that recyclability could be successfully achieved with consistent results up to the 6th cycle, after which the immobilised enzyme lost activity (as displayed in Figure 5).

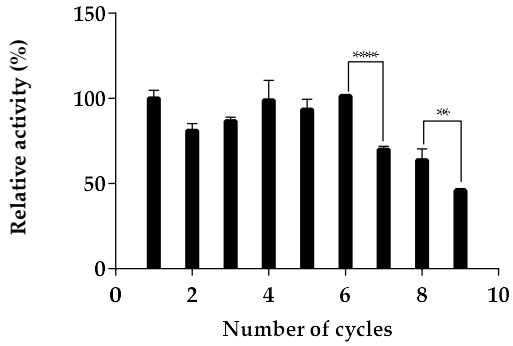

Figure 5. Recyclability test of endo-1,4-β-mannanase immobilised on chitosan using 0.5% (*w*/*v*) LBG as substrate (30 min, pH 5.0, 55 °C). Each value in the panel represents the means ± SD (n = 3). Relative absorbance (%) was used, with cycle 1 set as 100%. Key: **** (*p*-value < 0.0001); ** (*p*-value = 0.0096).

3.5. Utilisation of Immobilised Man26A on MOS Generation from SBM

The untreated SBM (Figure 6a) showed the presence of six distinctive peaks (Figure 6a, peaks A–F). The results from the analysis of hydrolysed 6% (*w*/*v*) SBM by the free and immobilised enzyme using HPLC-RID showed seven distinct peaks for the immobilised (Figure 6b) and free mannanase (Figure 6c). The average net reducing sugar concentrations, produced from the hydrolysis of SBM by the free and immobilised enzyme, were between 0.25 mg/mL and 0.45 mg/mL. From the untreated SBM (Figure 6a), no MOS could be confidently identified from the standards (M1–M6) (Figure 6a, peak A–F). Identical unidentifiable peaks were present in the hydrolysed samples (Figure 6b, peaks A–F and Figure 6c, peaks A–F). However, the hydrolysed SBM (Figure 6b,c) showed the presence of M2 (Figure 6b, peak G and Figure 6c, Peak G) and M1 (Figure 6b, peak H and Figure 6c, peak H) after hydrolysis with the relevant enzymes. These peaks were quantified using standard curves, showing ±0.35 mg/mL concentrations. The concentration of M1 was too low to be quantified from the standard curves for both enzyme hydrolysis samples.

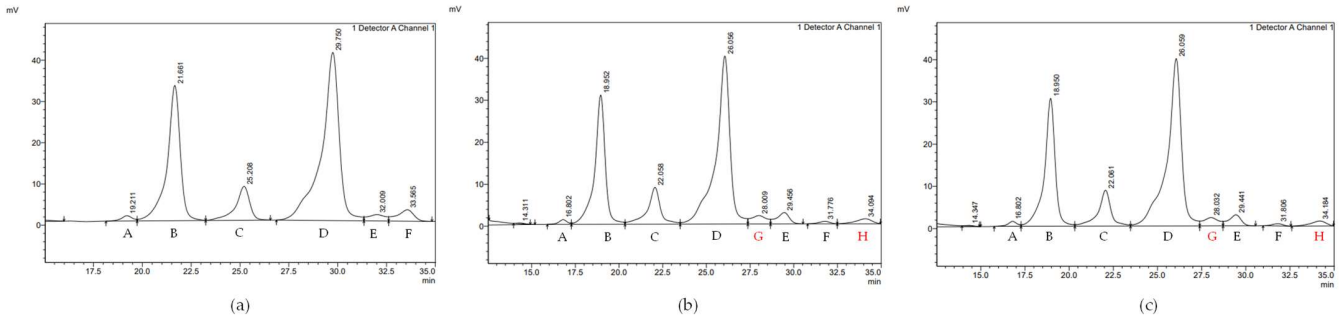

Figure 6. High-performance liquid chromatography analysis of (**a**) untreated 6% SBM, (**b**) hydrolysed 6% (*w*/*v*) SBM by immobilised endo-1,4-β-mannanase enzyme (9.14 U/mg), (**c**) hydrolysed 6% (*w*/*v*) free endo-1,4-β-mannanase enzyme (44.05 U/mg). Analysed using a Carbosep CHO 411 column, flow rate (0.26 mL/min), and a refractive index detector (RID). MOS standards were used to identify peaks of interest (M1–M6).

3.6. Prebiotic Effects of SBM-Derived MOS

The prebiotic potential of MOS produced by the hydrolysis of SBM with immobilised mannanases was evaluated. Figure 7 shows the cell viability (Figure 7a) and cell density (Figure 7b) of the probiotics as a result of cultivation in MOS, positive (glucose) and negative (no carbon source) controls.

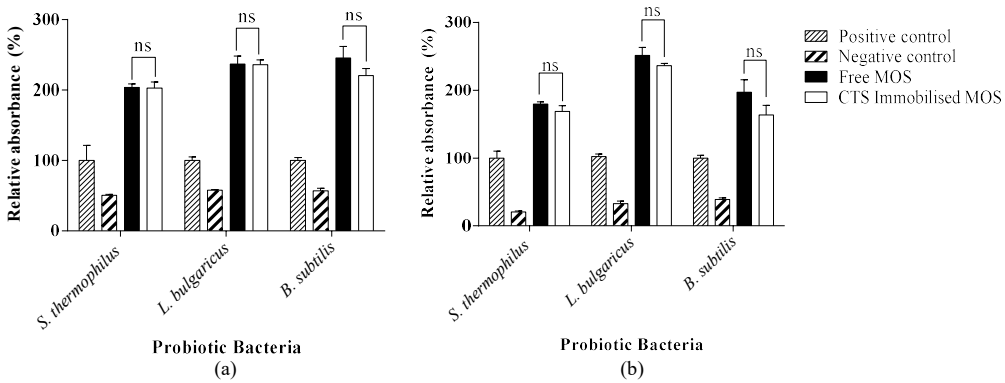

Figure 7. The evaluation of the prebiotic potential of SBM-generated sugars (0.155 mg/mL) produced using free and immobilised endo-β-1,4-mannanase by in vitro fermentation by probiotic bacteria (*Streptococcus thermophilus, Bacillus subtilis*, and *Lactobacillus bulgaricus*); (**a**) cell viability and (**b**) cell density. "ns" = Not significant.

The probiotic strains: *S. thermophilus*, *B. subtilis*, and *L. bulgaricus* showed a significant difference in cell viability when grown on the different carbon sources, with higher survival in the presence of SBM-produced sugars by the free and immobilised enzymes when compared to their positive control ($p = 0.0016$; $p < 0.0001$; $p = 0.0001$ and $p = 0.0012$; $p < 0.0001$; $p = 0.0001$, respectively) (Figure 7a). Similarly, the cell density study (Figure 7b) showed that probiotics amassed more cell mass in the presence of SBM-produced sugars over the positive control of glucose. These values showed a greatly significant difference for the probiotic strains *S. thermophilus, B. subtilis*, and *L. bulgaricus* of the free and immobilised enzymes compared to their positive controls ($p = 0.0008$; $p < 0.0001$; $p = 0.0018$; and $p = 0.0002$; $p < 0.0001$; $p = 0.0009$, respectively). The results confirmed that there was no significant difference in probiotic response, in reference to cell viability and cell density, for the SBM-produced sugars by the free and immobilised enzymes for the probiotics *S. thermophilus, B. subtilis,* and *L. bulgaricus* ($p = 0.8754$; $p = 0.9261$; 0.0902; and $p = 0.1096$; $p = 0.1049$; 0.06085, respectively).

4. Discussion

To promote a sustainable food production system, antibiotic alternatives such as prebiotic MOS are vital for producing healthy and nutritious poultry products [34]. The production of MOS from SBM was investigated using an immobilised mannanase to establish the feasibility of attempting to create a cheaper and more reusable reaction to benefit the poultry industry.

Enzyme immobilisation on glutaraldehyde-activated chitosan nanoparticles was investigated to develop a cost-effective strategy to enhance the enzymes' stability, activity, and recyclability [35]. After immobilisation, the immobilisation and activity yields were determined as 82.25% and 20.75%, respectively.

The FTIR spectra of Chitosan, A-CTS, and CTS (Figure 1) were established. Broad bands stretching between 3700cm^{-1} to 3000 cm^{-1} for the Chitosan, A-CTS, and CTS samples were attributed to O-H stretching vibrations. A shift in wavenumber was identified from 3276 cm^{-1} (Chitosan) to 3260 cm^{-1}(A-CTS) and then to 3206 cm^{-1} (CTS). This is due to a change in confirmation of the chitosan after glutaraldehyde activation and enzyme immobilisation [28]. A band at 2961cm^{-1} (Chitosan) shifted to 2967 cm^{-1} (A-CTS) and then 2987 cm^{-1} (CTS) with each step in the immobilisation procedure. This has been allocated to a C-H stretching region, prominent from the pyranose ring of chitosan [36,37]. The increase in wavenumber confirms the addition of C-H bonds to the A-CTS and CTS samples, likely caused by the activation of chitosan by glutaraldehyde and immobilisation of the endo-1,4-β-mannanase enzyme, respectively. The next prominent peak for the samples under investigation was distributed at 2915 cm^{-1} (Chitosan and A-CTS) and 2910 cm^{-1} (CTS)—this has been attributed to an N-H stretching region [28]. Evidence from the FTIR spectra confirms the activation of chitosan by glutaraldehyde. A band at 1730 cm^{-1} for the CTS and A-CTS confirmed the presence of a C=O within the structure. This band is absent in the untreated chitosan—indicating that the reaction with glutaraldehyde resulted in the addition of free aldehyde groups. The untreated chitosan sample experience two bands, absent in the A-CTS and CTS samples—distributed at 1642 cm^{-1} and 1604 cm^{-1}; these were attributed to the presence of an amide (NH_2) characteristically found within the chitosan structure [38–40]. This was previously seen by [40] and described as the asymmetric bending of -NH_2. The A-CTS and CTS samples saw an intensification and shift to the above-mentioned bands (1642 cm^{-1} and 1604 cm^{-1}) resulting in the formation of bands at 1681 cm^{-1} and 1687 cm^{-1}, and 1697 cm^{-1} and 1685 cm^{-1}, respectively. This shift was attributed to the formation of an Imine bond (C=N). This initially occurs because of the untreated chitosan (NH_2) binding to the free aldehyde of groups of glutaraldehyde (C=O), this otherwise being described as a Shiffs base formation [38–40]. The wavenumber is then slightly shifted for the CTS, which is attributed to additional imine bonds due to free aldehyde groups (C=O) binding to the free amide groups found on the surface of the endo-1,4-β-mannanase. The above evidence from FTIR confirms the activation of chitosan and immobilisation of the endo-1,4-β-mannanase by the formation of an imine bond (C=N) [28,39,40]. It has been previously stated in the literature that the formation of an imine bond by a reaction involving an amine and an aldehyde will result in a bond with covalent characteristics [41–44].

XRD analysis of untreated chitosan (Figure 2a) showed characteristic peaks of chitosan's crystalline structure at 2θ = 10.558° and 19.661°. These peaks have been identified frequently in the literature during XRD analysis of chitosan [44–46]. An additional peak was visible from the untreated chitosan sample, present at 2θ = 42.531°, this was confirmed by literature to be a common peak of untreated chitosan [46,47]. Analysis of the A-CTS sample showed a drastic drop in the intensity of the crystallinity peaks, with a slight shift in 2θ 19.661° peak to 18.032°, this being an attribute previously seen with the activation of chitosan by glutaraldehyde [48]. The XRD analysis of A-CTS (Figure 2b) confirmed the alteration of the chitosan by addition of glutaraldehyde. The drop in intensity between the untreated chitosan (Figure 2a) and the A-CTS (Figure 2b) is due to the formation of an amorphous structure. This is as a result of glutaraldehyde causing substitutions

within the chitosan's hydroxyl and amino groups, leading to the deformation of hydrogen bonds [46,48]. The CTS sample (Figure 2c) was analysed via XRD with supporting evidence of enzyme immobilization. Peak intensity remained low as a result of the previous activation of chitosan by glutaraldehyde. Several new peaks were formed, 2θ = 18.032°, 22.631°, 24.739°, 31.064°, 33.363°, 37.005°, 42.531°, 45.533°, 49.469°, and 51.569°—with peaks at 2θ = 18.032° and 42.531° remaining unchanged compared to the A-CTS XRD analysis (Figure 2b). The addition of new peaks confirms the strong binding of the endo-1,4-β-mannanase to the glutaraldehyde activated chitosan nanoparticles, like what was previously seen in literature [49].

The biochemical characteristics (Figure 3) of the free and immobilised mannanase on glutaraldehyde-activated chitosan nanoparticles were investigated. The free and immobilised enzymes' temperature optimum (Figure 3a) was established at 60 °C. This result has been observed previously, where endo-1,4-β-mannanase derived from *Clitocybe geotropa* immobilised on chitosan-coated magnetite nanoparticles was found to exhibit the same temperature optima for both the free and immobilised enzyme [50]. The thermostabilities of the enzymes in the current study were established (Figure 3b), where it was shown that both enzymes retained 100% activity over the first 6 h and, thereafter, retained 30% activity. This result was not expected, as immobilisation by crosslinking can increase enzyme stability [28,29]. The pH optima of the immobilised and free mannanase (Figure 3c) were pH 3 and pH 6, respectively. This finding is different to that of an immobilised and free mannanase from *Streptomyces* sp., which retained the same optimum pH value of 7.5 [28]. The reduced pH benefits the industrial industry as the chances of microbial contamination of the immobilised enzyme are reduced. This is a likely problem of long-term enzyme storage [51].

The kinetic parameters (Figure 4 and Table 1), obtained by non-linear regression of the Michaelis–Menten plot, showed that the K_M and V_{max} values of the enzymes were affected by the immobilisation procedure. Kinetic parameters were determined for the model substrate LBG (Figure 4a and Table 1) and the complex substrate under investigation, SBM (Figure 4b and Table 1). For LBG, a slightly lower K_M for the immobilised enzyme against the free enzyme could be attributed to either a change in the enzyme's conformation or to improved access of the substrate to the active sites of the enzymes [51]. This result showed that the immobilised enzyme had a slightly higher affinity for the LBG substrate than the free enzyme. The decrease in V_{max} after immobilisation shows that the efficiency of the enzyme to catalyse the reaction is lowered drastically after the immobilisation procedure. The results for V_{max} and K_M did not correlate with literature, as Dhiman and colleagues [52] obtained results which showed that the hydrolysis of LBG by a mannanase immobilised onto sodium-alginate beads displayed a lower affinity for the substrate than that of the free enzyme. The kinetic analysis with SBM contradicted that of the soluble substrate, LBG. The immobilised enzyme's affinity for the substrate (as shown by the K_M) was significantly higher than that of the free enzyme. This result was previously experienced by [49]. It was hypothesised to be due to an improved orientation of the enzyme, increasing accessibility to the active site by the substrate. However, this result was seen with LBG and not with an insoluble substrate such as SBM. The V_{max} showed that when the enzyme under question is hydrolysing an insoluble substrate such as SBM, the free and immobilised enzyme's catalytic efficiency acted similarly—displaying deficient catalytic ability compared to a soluble substrate.

The enzyme-immobilised chitosan nanoparticles were then assessed for their recyclability. In previous studies where an endo-1,4-β-mannanase derived from a *Streptomyces* species was immobilised on chitosan nanoparticles, an 83.6% activity yield was reported, providing evidence of the potential to increase activity with this method of immobilisation [28]. The recyclability study for the chitosan immobilisation (Figure 5) showed that the enzyme activity maintained a high reusability up to the 6th cycle, after which a decrease in activity was experienced. This shows great potential for a reusable mannanase formulation to produce prebiotic MOS.

The characterisation of the SBM-produced sugars, present with and without enzyme hydrolysis by free and immobilised enzymes, was performed by HPLC (Figure 6). The average net, reducing sugar concentration was between 0.25 mg/mL and 0.45 mg/mL for the free and immobilised enzymes, respectively. The identification of MOS residues from the standard curve showed that sugars were present within the untreated SBM sample; however, none of these sugars could be identified as MOS (Figure 6a, peak A–F). After hydrolysis, two distinct peaks were present (Figure 6b, peak G and H and Figure 6c, peak G and H); these were identified as M2 and M1, respectively. Quantifying the sugars produced after hydrolysis showed that approximately 0.35 mg/mL of the reducing sugars were M2, whilst M1 concentrations were too low to quantify using the generated standard curves.

The final aim of the study was to investigate the prebiotic potential of MOS with three probiotic strains: *S. thermophilus*, *B. subtilis*, and *L. bulgaricus.* The cell viability and cell density were tested to determine whether prebiotic MOS can stimulate the growth and metabolic activity of the probiotics under investigation [53]. The probiotic bacteria *B. subtilis* was investigated for its ability to utilise SBM-produced prebiotic sugars with great success. Studies through literature showed that *B. subtilis* contains a mannose utilisation locus (PUL) encoding for three factors contributing to the uptake and utilisation of mannose towards glycolysis—these include a transcriptional factor, a phosphotransferase system (PTS) mannose-specific enzyme, and mannose-6-phosphatase [53]. This information supports and confirms the obtained results of *B. subtilis* successfully utilising MOS in this study. The probiotic bacteria *Streptococcus thermophilus* was investigated for SBM-produced sugar utilisation, with results showing great success against the positive control of glucose. Within the research of transcriptional analysis of *Streptococcus mutans* [54], it was observed that an operon (SMU.1956 to -1961) within the phosphoenolpyruvate-sugar PTSs, was described to hold inducible fructose and mannose sugar-specific multiprotein permeases ($EII^{Fru/Man}$) in both the cytoplasm (EIIA and EIIB) and the membrane channel (EIIC), with transcription initiated in the presence of mannose [54]. Previous literature observed mannose to stimulate an induction response of up to 37-fold higher than mannitol-grown cells [54]. The *Streptococcus thermophilus* strain utilised the SBM-produced sugars efficiently—this information is supported by [54] and the *Streptococcus* strain's ability to induce transcription in the presence of mannose. According to literature, *Lactobacillus* species such as *Lactobacillus casei* possess the capability for mannose/fructose metabolism, a process regulated by LSEI_0681 [55]. However, the inhibition MOS utilisation will occur within a nutrient-deficient environment, resulting in the downregulation of LSEI_0681. In this study, the ability of the probiotics to access salt was not limited [55]; therefore, the results obtained for mannose utilisation are achievable. The immobilised enzyme displayed consistently higher results than the positive and negative control. This could be attributed to the utilisation of SBM-produced sugars by probiotic bacteria, but further research needs to be conducted to confirm this. The cell density was then tested—this describes how well the cells increased in mass in solution, but it cannot distinguish between dead or live cells. Optical densities for cell viability and cell density were closely related, confirming that no significant proportion of cell death occurred within the study for the SBM-produced sugars-stimulated probiotic strains.

5. Conclusions

It was confirmed via FTIR and XRD that an endo-1,4-β-mannanase derived from *A. niger* was immobilised on glutaraldehyde-activated chitosan nanoparticles by covalent attachment. The immobilised enzyme showed successful recyclability over six consecutive cycles, with a 50% drop in reusability after the 9th cycle. The physicochemical parameters of the immobilised and free enzyme showed that the optimum temperature (60 °C) and thermostability remained unchanged after the immobilisation procedure. However, the pH optimum of the immobilised enzyme (pH 2.0) became more acidic than the free enzyme (pH 6.0). The immobilised mannanase was then used to generate β-MOS from SBM, which were characterised by HPLC, showing the production of M2 as the major by-product

of SBM hydrolysis. The prebiotic potential of SBM-produced sugars showed improved cellular growth and viability of probiotic bacteria compared to glucose as a carbon source. This study supported that immobilised mannanase can be used for sustainable prebiotic production from mannan-containing agricultural feedstocks.

Author Contributions: Conceptualisation, A.S.A., L.M., S.M., N.K. and B.I.P.; methodology, A.S.A.; validation, A.S.A., L.M., S.M., N.K. and B.I.P.; formal analysis, A.S.A.; data curation, A.S.A.; writing—original draft preparation, A.S.A. and L.M.; writing—review and editing, A.S.A., L.M., S.M., N.K. and B.I.P.; supervision, L.M., S.M. and B.I.P.; project administration, B.I.P.; funding acquisition, B.I.P. All authors have read and agreed to the published version of the manuscript.

Funding: The work was funded by Rhodes University's Research Council (RC) grant and a Rated Researcher Grant (RRG).

Informed Consent Statement: Not applicable.

Data Availability Statement: Not applicable.

Conflicts of Interest: The authors declare no conflict of interest.

References

1. Jana, U.K.; Kango, N.; Pletschke, B.I. Hemicellulose-derived oligosaccharides: Emerging prebiotics in disease alleviation. *Front. Nutr.* **2021**, *8*, 670817. [CrossRef] [PubMed]
2. Yasmin, A.; Butt, M.S.; Afzaal, M.; van Baak, M.; Nadeem, M.T.; Shahid, M.Z. Prebiotics, gut microbiota and metabolic risks: Unveiling the relationship. *J. Funct. Foods* **2015**, *17*, 189–201. [CrossRef]
3. Yu, X.; Yin, J.; Li, L.; Luan, C.; Zhang, J.; Zhao, C.; Li, S. Prebiotic potential of Xylooligosaccharides derived from corn cobs and their *in vitro* antioxidant activity when combined with *Lactobacillus*. *Microbiol. Biotechnol.* **2015**, *25*, 1084–1092. [CrossRef] [PubMed]
4. Hlalukana, N.; Magengelele, M.; Malgas, S.; Pletschke, B.I. Enzymatic conversion of mannan-rich plant waste biomass into prebiotic mannooligosaccharides. *Foods* **2021**, *10*, 2010. [CrossRef]
5. Xiao, R.; Power, R.F.; Mallonee, D.; Rout, K.; Spangler, L.; Pescatore, A.J.; Cantor, A.H.; Ao, T.; Pierce, J.L.; Dawson, K.A. Effects of yeast cell wall-derived mannanoligosaccharides on jejunal gene expression in young broiler chickens. *Poult. Sci. J.* **2012**, *91*, 1660–1669. [CrossRef]
6. Che, T.; Song, M.; Liu, Y.; Johnson, R.; Kelley, K.; Van Alstine, W.; Dawson, K.; Pettigrew, J. Mannan oligosaccharide increases serum concentrations of antibodies and inflammatory mediators in weanling pigs experimentally infected with porcine reproductive and respiratory syndrome virus. *Anim. Sci. J.* **2012**, *90*, 2784–2793. [CrossRef]
7. Garcia Diaz, T.; Ferriani Branco, A.; Jacovaci, F.A.; Cabreira Jobim, C.; Pratti Daniel, J.L.; Iank Bueno, A.V.; Gonçalves Ribeiro, M. Use of live yeast and mannanoligosaccharides in grain-based diets for cattle: Ruminal parameters, nutrient digestibility, and inflammatory response. *PLoS ONE* **2018**, *13*, e0207127.
8. Malgas, S.; van Dyk, S.J.; Pletschke, B.I. β-Mannanase (Man26A) and α-galactosidase (Aga27A) synergism—A key factor for the hydrolysis of galactomannan substrates. *Enzym. Microb. Technol.* **2015**, *70*, 1–8. [CrossRef]
9. Sharma, P.; Sharma, S.; Ramakrishna, G.; Srivastava, H.; Gaikwad, K. A comprehensive review on leguminous galactomannans: Structural analysis, functional properties, biosynthesis process and industrial applications. *Crit. Rev. Food Sci. Nutr.* **2020**, *62*, 443–465. [CrossRef]
10. Hsiao, H.Y.; Anderson, D.M.; Dalet, N.M. Levels of β-mannan in soybean meal. *Poult. Sci. J.* **2006**, *85*, 1430–1432. [CrossRef]
11. Caldas, J.V.; Vignale, K.; Boonsinchai, N.; Wang, J.; Putsakum, M.; England, J.A.; Coon, C.N. The effect of β-mannanase on nutrient utilization and blood parameters in chicks fed diets containing soybean meal and guar gum. *Poult. Sci. J.* **2018**, *97*, 2807–2817. [CrossRef] [PubMed]
12. Shastak, Y.; Ader, P.; Feuerstein, D.; Ruehle, R.; Matuschek, M. ß-Mannan and mannanase in poultry nutrition. *Poult. Sci. J.* **2015**, *71*, 161–174. [CrossRef]
13. Saeed, M.; Ayasan, T.; Alagawany, M.; El-Hack, M.E.A.; Abdel-Latif, M.A.; Patra, A.K. The role of ß-mannanase (Hemicell) in improving poultry productivity, health and environment. *Braz. J. Poult. Sci.* **2019**, *21*, 1–8. [CrossRef]
14. White, D.; Adhikari, R.; Wang, J.; Chen, C.; Lee, J.H.; Kim, W.K. Effects of dietary protein, energy and β-mannanase on laying performance, egg quality, and ileal amino acid digestibility in laying hens. *Poult. Sci. J.* **2021**, *100*, 101312. [CrossRef] [PubMed]
15. Singh, S.; Singh, G.; Arya, S.K. Mannans: An overview of properties and application in food products. *Int. J. Biol. Macromol.* **2018**, *119*, 79–95. [CrossRef] [PubMed]
16. Sharma, K.; Dhillon, A.; Goyal, A. Insights into structure and reaction mechanism of β-mannanases. *Curr. Protein Pept. Sci.* **2018**, *19*, 34–47. [CrossRef]
17. Jana, U.K.; Kango, N. Characteristics and bioactive properties of mannooligosaccharides derived from agro-waste mannans. *Int. J. Biol. Macromol.* **2020**, *149*, 931–940. [CrossRef]

18. Suryawanshi, R.K.; Kango, N. Production of mannooligosaccharides from various mannans and evaluation of their prebiotic potential. *Food Chem.* **2021**, *334*, 127428. [CrossRef]
19. Homaei, A.A.; Sariri, R.; Vianello, F.; Stevanato, R. Enzyme immobilization: An update. *J. Chem. Biol.* **2013**, *6*, 185–205. [CrossRef]
20. Raghuvanshi, S.; Gupta, R. Advantages of the immobilization of lipase on porous supports over free enzyme. *Protein Pept. Lett.* **2010**, *17*, 1412–1416. [CrossRef]
21. Kumar, G.; Mudhoo, A.; Sivagurunathan, P.; Nagarajan, D.; Ghimire, A.; Lay, C.-H.; Lin, C.-Y.; Lee, D.-J.; Chang, J.-S. Recent insights into the cell immobilization technology applied for dark fermentative hydrogen production. *Bioresour. Technol.* **2016**, *219*, 725–737. [CrossRef] [PubMed]
22. Verma, M.L.; Kumar, S.; Das, A.; Randhawa, J.S.; Chamundeeswari, M. Chitin and chitosan-based support materials for enzyme immobilization and biotechnological applications. *Environ. Chem. Lett.* **2020**, *18*, 315–323. [CrossRef]
23. Nunes, Y.L.; de Menezes, F.L.; de Sousa, I.G.; Cavalcante, A.L.G.; Cavalcante, F.T.T.; da Silva Moreira, K.; de Oliveira, A.L.B.; Mota, G.F.; da Silva Souza, J.E.; de Aguiar Falcão, I.R.; et al. Chemical and physical chitosan modification for designing enzymatic industrial biocatalysts: How to choose the best strategy? *Int. J. Biol. Macromol.* **2021**, *181*, 1124–1170. [CrossRef] [PubMed]
24. Barbosa, O.; Ortiz, C.; Berenguer-Murcia, Á.; Torres, R.; Rodrigues, R.C.; Fernandez-Lafuente, R. Glutaraldehyde in bio-catalysts design: A useful crosslinker and a versatile tool in enzyme immobilization. *RSC Adv.* **2014**, *4*, 1583–1600. [CrossRef]
25. Elchinger, P.H.; Delattre, C.; Faure, S.; Roy, O.; Badel, S.; Bernardi, T.; Taillefumier, C.; Michaud, P. Immobilization of proteases on chitosan for the development of films with anti-biofilm properties. *Int. J. Biol. Macromol.* **2015**, *72*, 1063–1068. [CrossRef]
26. Bonazza, H.L.; Manzo, R.M.; dos Santos, J.C.S.; Mammarella, E.J. Operational and thermal stability analysis of *Thermomyces lanuginosus* lipase covalently immobilized onto modified chitosan supports. *Appl. Biochem. Biotechnol.* **2018**, *184*, 182–196. [CrossRef]
27. Patel, K.K.; Tripathi, M.; Pandey, N.; Agrawal, A.K.; Gade, S.; Anjum, M.M.; Tilak, R.; Singh, S. Alginate lyase immobilized chitosan nanoparticles of ciprofloxacin for the improved antimicrobial activity against the biofilm associated mucoid *P. aeruginosa* infection in cystic fibrosis. *Int. J. Pharm.* **2019**, *563*, 30–42. [CrossRef]
28. Mohapatra, B.R. Characterization of β-mannanase extracted from a novel *Streptomyces* species Alg-S25 immobilized on chitosan nanoparticles. *Biotechnol. Biotechnol. Equip.* **2021**, *35*, 150–161. [CrossRef]
29. Blibech, M.; Chaari, F.; Bhiri, F.; Dammak, I.; Ghorbel, R.E.; Chaabouni, S.E. Production of manno-oligosaccharides from locust bean gum using immobilized *Penicillium occitanis* mannanase. *J. Mol. Catal. B Enzym.* **2011**, *73*, 111–115. [CrossRef]
30. Bradford, M.M. A rapid and sensitive method for the quantitation of microgram quantities of protein utilizing the principle of protein-dye binding. *Anal. Biochem.* **1976**, *72*, 248–254. [CrossRef]
31. Miller, G.L. Use of dinitrosalicyclic acid reagent for determination of reducing sugars. *Anal. Chem.* **1959**, *31*, 426–428. [CrossRef]
32. Britton, H.T.S.; Robinson, R.A. Universal buffer solutions and the dissociation constant of veronal. *J. Chem. Soc.* **1931**, *1*, 456–1462. [CrossRef]
33. Magengelele, M.; Hlalukana, N.; Malgas, S.; Rose, S.H.; van Zyl, W.H.; Pletschke, B.I. Production and in vitro evaluation of prebiotic manno-oligosaccharides prepared with a recombinant *Aspergillus niger* endo-mannanase, Man26A. *Enzym. Microb. Technol.* **2021**, *150*, 109893. [CrossRef] [PubMed]
34. Manyi-Loh, C.; Mamphweli, S.; Meyer, E.; Okoh, A. Antibiotic use in agriculture and its consequential resistance in environmental sources: Potential public health implications. *Molecules* **2018**, *23*, 795. [CrossRef] [PubMed]
35. Alnadari, F.; Xue, Y.; Zhou, L.; Hamed, Y.S.; Taha, M.; Foda, M.F. Immobilization of β-glucosidase from *Thermatoga maritima* on chitin-functionalized magnetic nanoparticle via a novel thermostable chitin-binding domain. *Sci. Rep.* **2020**, *10*, 1663. [CrossRef] [PubMed]
36. Baroudi, A.; García-Payo, C.; Khayet, M. Structural, mechanical, and transport properties of electron beam-irradiated chitosan membranes at different doses. *Polym. J.* **2018**, *10*, 117. [CrossRef]
37. Mahamed, S.A.; Al-Malki, A.L.; Kumosani, T.A. Horseradish peroxidase and chitosan: Activation, immobilization and comparative results. *Int. J. Biol. Macromol.* **2013**, *60*, 295–300. [CrossRef]
38. Gűr, S.D.; İdil, N.; Aksöz, N. Optimization of enzyme co-immobilization with sodium alginate and glutaraldehyde-activated chitosan beads. *Appl. Biochem. Biotechnol.* **2018**, *184*, 538–552. [CrossRef]
39. Klein, M.P.; Nunes, M.R.; Rodigues, R.C.; Benvenutti, E.V.; Costa, T.M.H.; Hertz, P.F.; Ninow, J.L. Effect of the support size on the properties of β-galactosidase immobilized on chitosan: Advantages and disadvantages of macro and nanoparticles. *Biomacromolecules* **2012**, *13*, 2456–2464. [CrossRef]
40. Collins, S.E.; Lassalle, V.; Ferreira, M.L. FTIR-ATR characterization of free *Rhizomucor meihei* lipase (RML), Lipozyme RM, IM and chitosan-immobilized RML. *J. Mol. Catal. B Enzym.* **2011**, *72*, 220–228. [CrossRef]
41. Belowicha, M.E.; Stoddart, J.F. Dynamic Imine Chemistry. *Chem. Soc. Rev.* **2012**, *41*, 2012. [CrossRef] [PubMed]
42. Ciaccia, M.; Cacciapaglia, R.; Mencarelli, P.; Manolini, L.; Stefano, S.D. Fast Transimination in organic solvents in the absence of proton and metal catalysts. A key to iminemetathesis catalyzed by primary amines under mind conditions. *Chem. Sci.* **2013**, *5*, 2253–2261. [CrossRef]
43. Dai, W.; Shao, F.; Szczerbiński, J.; McCaffrey, R.; Zenobi, R.; Jin, Y.; Schlüter, A.D.; Zhang, W. Synthesis of a Two-Dimensional Covalent Organic Monolayer through Dynamic Imine Chemistry at the Air/Water Interface. *Angew. Chem. Int. Ed.* **2016**, *55*, 213–217. [CrossRef]

44. Morsy, M.; Mostafa, K.M.; Amyn, H.A.M.; El-Ebissy, A.A.H.; Salah, A.M.; Youssef, M.A. Synthesis and characterization of free dryer chitosan nanoparticles as multifunctional eco-friendly finish for fabricating easy care and antibacterial cotton textiles. *Egypt. J. Chem.* **2019**, *62*, 1277–1293.
45. Kumar, S.; Koh, J. Physiochemical, Optical and biological activity of chitosan-chrome derivative for biomedical applications. *Int. J. Mol. Sci.* **2012**, *13*, 6102–6116. [CrossRef] [PubMed]
46. Galan, J.; Trilleras, J.; Zapata, P.A.; Arana, V.A.; Grande-Tovar, C.D. Optimization of chitosan glutaraldehyde-crosslinked beads for reactive blue 4 anionic dye removal using a surface response methodology. *Life* **2021**, *11*, 85. [CrossRef]
47. Garnica-Palafox, I.M.; Sánchez-Arévalo, F.M. Influence of natural and synthetic crosslinking reagents on the structural and mechanical properties of chitosan-based hybrid hydrogels. *Carbohydr. Polym.* **2016**, *151*, 1073–1081. [CrossRef]
48. Li, B.; Shan, C.L.; Zhou, Q.; Fang, Y.; Wang, Y.L.; Xu, F.; Han, L.R.; Ibrahim, M.; Guo, L.B.; Xie, G.L.; et al. Synthesis, characterisation, and antibacterial activity of cross-linked chitosan-glutaraldehyde. *Mar. Drugs* **2013**, *11*, 1534–1552. [CrossRef]
49. Sadaqat, B.; Sha, C.; Dar, M.A.; Dhanavade, M.J.; Sonawane, K.D.; Mohamed, H.; Shao, W.; Song, Y. Modifying thermostability and reusability by immobilization on glutaraldehyde cross-linked chitosan beads. *Biomolecules* **2022**, *12*, 999. [CrossRef]
50. Nadaroglu, H.; Sonmez, Z. Purification of an endo-beta-1,4-mannanase from *Clitocybe geotropa* and immobilisation on chitosan-coated magnetite nanoparticles: Application for fruit juices. *Dig. J. Nanomater. Biostruct.* **2016**, *11*, 685–697.
51. Rebroš, M.; Rosenberg, M.; Mlichova, Z.; Kristofikova, L. Hydrolysis of sucrose by invertase entrapped in polyvinyl alcohol hydrogel capsule. *Food Chem.* **2007**, *102*, 784–787. [CrossRef]
52. Dhiman, S.; Srivastava, B.; Singh, G.; Khatri, M.; Arya, S.K. Immobilization of mannanase on sodium alginate-grafted-β-cyclodextrin: An easy and cost effective approach for the improvement of enzyme properties. *Int. J. Biol. Macromol.* **2019**, *156*, 1347–1358. [CrossRef] [PubMed]
53. Suhaibani, A.A.; Bacha, A.B.; Alonazi, M.; Bhat, R.S.; El-Ansary, A. Testing the combined effects of probiotics and prebiotics against neurotoxic effects of propionic acid orally administered to rat pups. *Food Sci. Nutr.* **2021**, *9*, 4440–4451. [CrossRef] [PubMed]
54. Ajdić, D.; Pham, V.T.T. Global transcription analysis of *Streptococcus mutans* sugar transporters using microarrays. *J. Bacteriol.* **2007**, *189*, 5049–5059. [CrossRef]
55. Licandro-Seraut, H.; Scornec, H.; Pédron, T.; Cavin, J.F.; Sansonetti, P. Functional genomics of *Lactobacillus casei* establishment in the gut. *Proc. Natl. Acad. Sci. USA* **2014**, *111*, 3101–3109. [CrossRef]